Journal of Materials Chemistry C

ROYAL SOCIETY OF CHEMISTRY

PAPER

View Article Online
View Journal | View Issue

Cite this: J. Mater. Chem. C, 2023, 11, 8037

Aggregation effects on the one- and two-photon excited fluorescence performance of regioisomeric anthraquinone-substituted perylenediimide†

Liang Xu, *[a] Xueting Long,[a] Jiaxin He,[a] Lingxiu Liu,[b] Fangyuan Kang,[c] Ziqi Deng,[d] Jieyu Wu,[e] Xiao-Fang Jiang,[e] Jianguo Wang *[b] and Qichun Zhang *[cf]

Received 18th September 2022,
Accepted 7th October 2022

DOI: 10.1039/d2tc03928a

rsc.li/materials-c

Regioisomerism is an efficient strategy for finely tuning the structures of molecules in the isolated or the aggregated state. Herein, two regioisomers of perylene diimide (PDI) derivatives have been designed and synthesized. The positions of the substituent anthraquinone groups display distinct influences on their molecular conformation and aggregate structures, resulting in different fluorescence properties upon one- and two-photon excitation. In addition, owing to the bright emission, cellular imaging tests based on their nanoparticles were also conducted.

Introduction

Organic luminescent materials have drawn considerable attention owing to many attractive advantages, such as the diversity of molecular design, high compatibility with organisms, and potential to prepare flexible devices.[1] Therefore, they have great potential for applications in biological imaging,[2–5] organic nonlinear optical (NLO) materials,[6–10] *etc*. The performance of these materials depends on not only the properties of the well-designed molecules with specific functional groups but also their aggregate states.[11–13] In 2001, Tang and co-workers first coined the concept of aggregation-induced emission (AIE).[14] In 2018, Li and co-workers first coined the concept of molecular uniting set identified characteristic (MUSIC).[15] In 2020, Tang and co-workers put forward the concept of "aggregate science".[16] These concepts all highlight the key role of molecular aggregates in the performance of organic luminescent materials.

There are mainly two approaches used to adjust the molecular aggregates. One is external force, including the characteristics of solvent (polarity, viscosity, hydrophilia or hydrophobicity), mechanical force, light, and electric field.[17] For instance, polymorphs,[18,19] mechanoluminescence (ML),[20–23] photoinduced room temperature phosphorescence (RTP),[24–28] and the optimized nonlinear optical (NLO) properties were achieved after electric poling.[29–35] The other is internal force including π–π stacking, anion–π interactions, dispersion forces, electrostatic interactions and hydrogen bonding.[36,37] For instance, alkyl chains can suppress molecular motions and favour the RTP properties through the formation of multiple C–H···π and C–H···X (X presents heteroatoms such as N, O, S, *etc.*) interactions with surrounding aromatic rings or heteroatoms.[38,39] Moreover, the different lengths of alkyl chains can subtly tune intermolecular interactions, resulting in a unique oddeven effect in photoluminescence.[40,41] Hydrogen bonding induced by hydroxy, carboxylic acid and amino moieties can promote RTP performance by suppressing the molecular motions in the aggregated states.[42] Overall, predesign or modification of the molecular aggregates at the stage of molecular design would be ideal, despite its great difficulty and challenges.

As one kind of molecular design method, regioisomerism is a very promising strategy for adjusting the molecular aggregates. In this way, a simple structural modification may drastically influence the luminescence properties of the molecular aggregates.[43] In recent three years, several groups have reported the use of regioisomerism to finely tune the structures of the molecular aggregates, leading to distinct luminescence

[a] Department of Chemistry and Key Laboratory for Preparation and Application of Ordered Structural Materials of Guangdong Province, Shantou University, Guangdong 515063, China. E-mail: xuliang@stu.edu.cn
[b] College of Chemistry and Chemical Engineering, Inner Mongolia Key Laboratory of Fine Organic Synthesis, Inner Mongolia University, Hohhot 010021, P. R. China. E-mail: wangjg@iccas.ac.cn
[c] Department of Materials Science and Engineering, City University of Hong Kong, Kowloon, Hong Kong SAR, China. E-mail: qiczhang@cityu.edu.hk
[d] Department of Chemistry, University of Hong Kong, Hong Kong, China
[e] Laboratory of Quantum Engineering and Quantum Material, School of Physics and Telecommunication Engineering, South China Normal University, Guangzhou 510006, China
[f] Center of Super-Diamond and Advanced Films (COSDAF), City University of Hong Kong, Hong Kong SAR, 999077, P. R. China

† Electronic supplementary information (ESI) available. See DOI: https://doi.org/10.1039/d2tc03928a

properties. In 2019, Li and co-workers reported a series of halogen-substituted triphenylamines. Among these, *ortho*-substituted products are all ML-inactive, while *meta*-substituted products are all ML-active.[44] In 2020, Wang, Zhang and co-workers reported a phenyl-substituted effect in tetraphenylpyrazine. They found that the *ortho*-phenyl substitution stimulates the AIE characteristics, but substituting at either *meta* or *para* position results in non-AIE active compounds.[45] In 2020, Tang, Lu, Qian and co-workers reported two triphenylamine-substituted dithienobenzophenazine and found that the *end*-substituted product is dominated by the ACQ properties while the *bay*-substituted product is AIE-active.[46] In 2020, Promarak and co-workers reported two *n*-hexylthiophene-substituted naphthothiadiazole with AIE properties. Due to a large steric repulsion between naphthothiadiazole and nearby thiophenes, the molecular conformation of the product substituted at the 3-position of thiophene is more twisted than that of the product substituted at the 4-position of thiophene. As a result, their fluorescence emission peak and quantum yields are totally different in solution and aggregate.[47] In 2020, Iyer and co-workers reported two pyridine-substituted triphenylethylene. When the pyridine group is substituted at the *ortho* position of the phenyl ring, the product is non-AIE active. When the pyridine group is substituted at the *para* position of the phenyl ring, the product is AIE active.[48] In 2021, Wang, Zhi and co-workers reported three aldehyde-substituted tetraaryl ethylenes. They are all AIE-active; however, the AIE amplification factors are totally different. The biggest one is 176.4 for the *para*-substituted product, while the smallest one is only 9.3 for the *meta*-substituted product.[49]

Although perylene diimides (PDIs) are one class of the most explored organic fluorescent materials, the report of the regioisomerism effect on the aggregate emission properties of PDIs is still rare. Tang, Sun and co-workers reported two tetraphenyl ethene-substituted PDIs with AIE properties.[50] The AIE amplification factor of the 1,7-substituted product is larger than that of the 1,6-substituted product. In 2021 and 2022, our group reported *bay*- and *ortho*-substituted PDIs with the benzanthrone or anthracene groups as the electron-donating moieties.[51,52] Very interesting phenomena are observed. With the substitution position of benzanthrone changing from *bay* to *ortho*, ACQ-to-AIE conversion is achieved. With the substitution position of anthracene changing from *bay* to *ortho*, the AIE process is accelerated and the AIE amplification factor is also enhanced.[51,52] However, it is still unknown what will happen if changing the substitution position of electron-withdrawing groups from *bay* to *ortho* on PDI.

Inspired by the above points, this work aims to explore the aggregate emission of PDIs with electron-withdrawing anthraquinone groups as the *bay*- and *ortho*-substituents. It is anticipated that by changing the anthraquinone group from the *ortho* position to the *bay* position of PDI, the resultant steric hindrance may alter the π-conjugated core and affect the molecular aggregates, which may make possible altering the aggregate fluorescence emission properties. Herein, we present the syntheses, UV-Vis absorption and fluorescence emission properties, femtosecond and nanosecond transient absorption properties, two-photon absorption properties, and theoretical calculations in detail. Finally, given the high fluorescence quantum yields of the products, their nanoparticles are also applied for cellular imaging.

Results and discussion

UV-Vis absorption and fluorescence emission spectra

As shown in Fig. 1, the UV-Vis absorption spectrum of PDI in THF shows three main peaks centered at 522, 486 and 455 nm, respectively. The *ortho*-substituted product *O*-PDI-ANQ in THF also exhibits structured absorption peaks centered at 524, 488 and 457 nm, respectively. The *bay*-substituted product *B*-PDI-ANQ in THF exhibits absorption peaks centered at 530 and 495 nm, respectively. Upon excitation at 525 nm, PDI shows vibronically resolved emission peaks centered at 530, 571 and 620 nm. *O*-PDI-ANQ exhibits slightly red-shifted emission peaks centered at 535, 576 and 625 nm. *B*-PDI-ANQ exhibits a broad emission band centered at 567 nm. As a result, the Stokes shifts for PDI, *O*-PDI-ANQ and *B*-PDI-ANQ are 8, 11 and 37 nm, respectively. It is worth noting that both the absorption and emission spectra of *B*-PDI-ANQ appear to be less structured in comparison to those of *O*-PDI-ANQ. For *O*-PDI-ANQ, the structured emission spectrum and small Stokes shift reflect its molecular rigidity. For *B*-PDI-ANQ, the extremely broad emission spectrum and the large Stokes shift suggest a drastic rearrangement of this flexible molecule in the excited state.[53] The optimized molecular structures in vacuum indeed reveal that the dihedral between the ANQ group and PDI core changes by 12° from the ground state to the excited state for

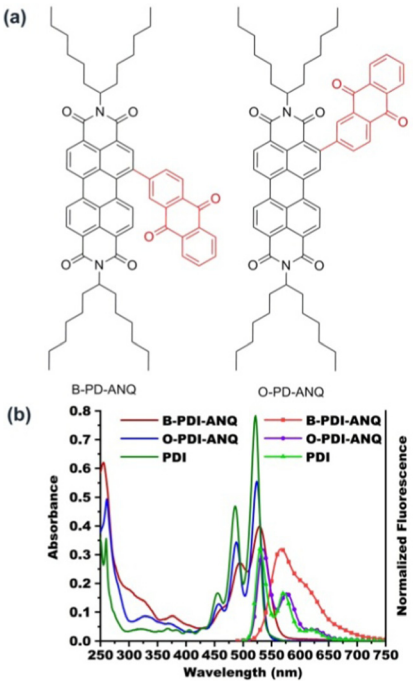

Fig. 1 (a) The molecular structures of *B*-PDI-ANQ and *O*-PDI-ANQ and (b) UV-Vis absorption and normalized fluorescence emission spectra of PDI, *B*-PDI-ANQ and *O*-PDI-ANQ in THF.

B-PDI-ANQ, while that is only 6° for *O*-PDI-ANQ (Fig. S5 and S6, ESI†). Using rhodamine B (Φ_F = 97% in ethanol) as the calibration standard, the fluorescence quantum yields (Φ_F) of PDI, *O*-PDI-ANQ and *B*-PDI-ANQ are 70, 70, and 54%, respectively. Partial reduction in the Φ_F value of *B*-PDI-ANQ when compared with PDI and *O*-PDI-ANQ could be attributed to the non-radiative decay pathways arising from the *bay* substitution of the PDI core.

Femtosecond and nanosecond transient absorption of *B*-PDI-ANQ and *O*-PDI-ANQ in THF

Further insights into the excited state deactivation in *bay*- and *ortho*-substituted PDI derivatives come from femtosecond and nanosecond transient absorption measurements. Fig. 2a–d show four distinct processes for *B*-PDI-ANQ after photoexcitation. First, *B*-PDI-ANQ exhibits two negative peaks centered at 534 and 493 nm corresponding to ground-state bleaching (GSB),[54] where one negative peak centered at 566 corresponds to stimulated emission (SE),[55] and two positive peaks centered at 345 and 710 nm come from excited-state absorption (ESA).[56] Second, the decrease of GSB signals at 534 nm suggests the occurrence of intramolecular charge transfer (ICT),[57] and no significant spectral shift is observed. It indicates that this singlet excited state with ICT character is formed very fast. Third, the transient absorption peaks do not show any change. This is probably due to the solvent rearrangement (SR).[58] Fourth, GSB and ESA signals gradually fall down to the baseline and remain at a 534 nm peak, which do not disappear even after reaching the maximum delay time of the fs-TA instrument (7.5 ns). This reveals that an intersystem crossing (ISC)[59] may take place to generate a triplet state. Compared to the fs-TA spectrum of *B*-PDI-ANQ, that of *O*-PDI-ANQ displays apparently different features. As shown in Fig. 2f, *O*-PDI-ANQ shows GSB at 532, 487, and 456 nm, SE at 576 nm and ESA at 345 and 706 nm. The SE feature of *O*-PDI-ANQ is more prominent than that of *B*-PDI-ANQ, which is consistent with the larger Φ_F value of *O*-PDI-ANQ. As shown in Fig. 2g, the SR feature persists in the transient spectra, but there is no ICT feature observed for *O*-PDI-ANQ. Therefore, there are two non-radiative decay processes (ICT and ISC) for the excited state of *B*-PDI-ANQ. In contrast, there is one non-radiative decay process (ISC) for the excited state of *O*-PDI-ANQ. This is the reason that the Φ_F value of *O*-PDI-ANQ is higher than that of *B*-PDI-ANQ. To obtain the exact rate constants of the excited state dynamics, the kinetic fittings of 534 nm for *B*-PDI-ANQ and 532 nm for *O*-PDI-ANQ are extracted from the data of fs-TA. As shown in Fig. 2e, for *B*-PDI-ANQ, the 534 nm transient absorption should be fitted by the four exponential functions, resulting in four lifetimes for them. The four lifetimes are τ_1 = 0.45 ps (16.2%), τ_2 = 6.5 ps (13.1%), τ_3 = 231 ps (12%),

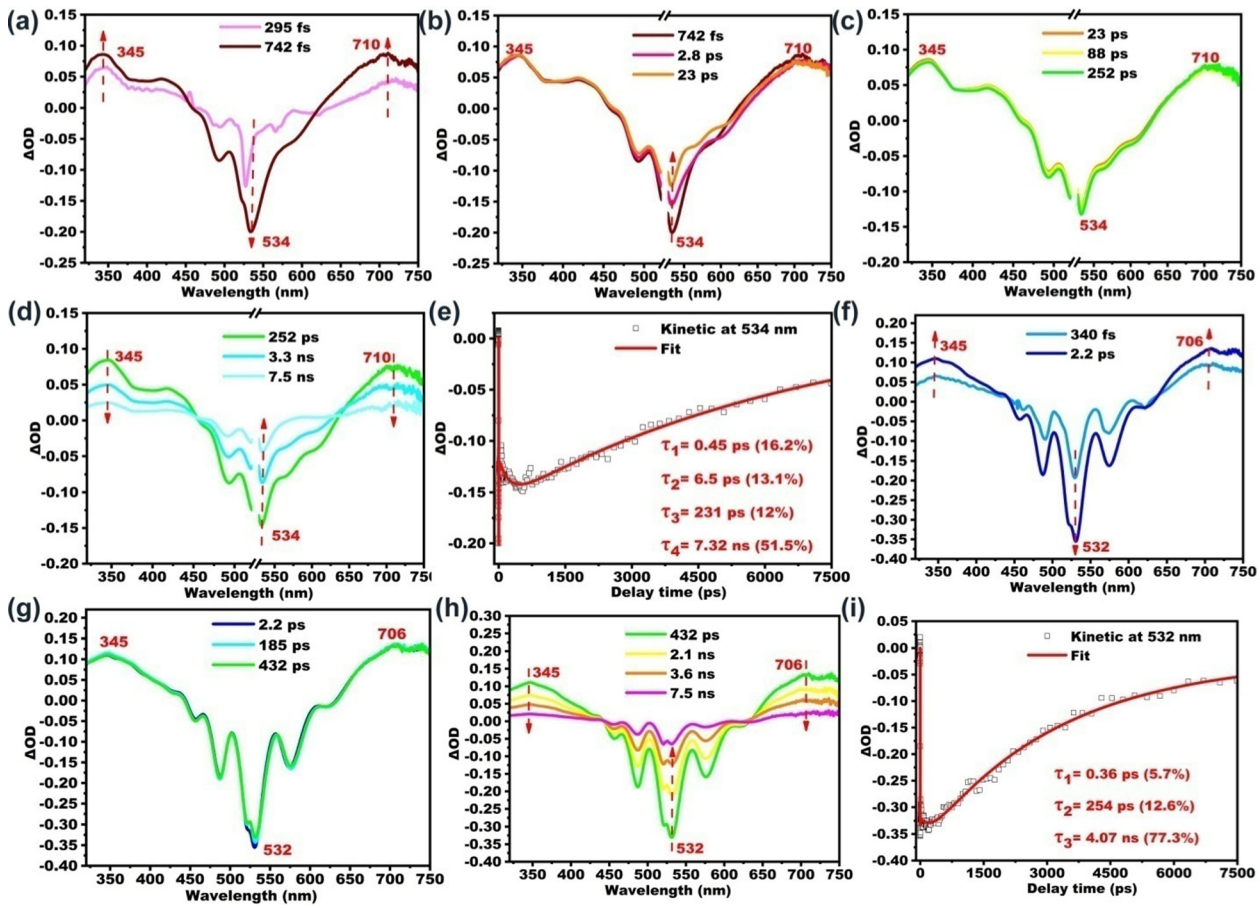

Fig. 2 Fs-TA spectra and kinetics of (a–e) *B*-PDI-ANQ and (f–i) *O*-PDI-ANQ in THF.

and τ_4 = 7.32 ns (51.5%), respectively. As shown in Fig. 2i, for *O*-PDI-ANQ, the 532 nm transient absorption should be fitted by the three exponential functions, resulting in τ_1 = 0.36 ps (5.7%), τ_2 = 254 ps (12.6%) and τ_3 = 4.07 ns (77.3%), respectively. To further confirm the generation of triplet states for *B*-PDI-ANQ and *O*-PDI-ANQ, purged nitrogen and oxygen experiments for nanosecond transient absorption (ns-TA) were performed. The results and discussion are available in the ESI.†

One-photon excited fluorescence properties

In order to investigate the fluorescence properties of *B*-PDI-ANQ and *O*-PDI-ANQ in their aggregated state, the fluorescence spectra of these compounds are measured in THF containing various water volume fractions (f_w). As shown in Fig. 3, the fluorescence intensities of *B*-PDI-ANQ are dramatically decreased at the initial stage from f_w = 0 to 30%, indicating a grave quenching effect. Unlike *B*-PDI-ANQ, the fluorescence intensities of *O*-PDI-ANQ have a very small decrease when f_w is below 60%, manifesting a slight quenching effect. When water is progressively added, an evident decrease in the fluorescence intensity of *O*-PDI-ANQ is observed at f_w = 70%.

In order to further clarify the quenching characteristics of *B*-PDI-ANQ and *O*-PDI-ANQ with the increase in the water content in the solution, the changes in the Φ_F values and the maximum emission wavelengths are plotted against the water fraction in the THF solutions. The quenching factor Φ_q is calculated by using the equation of $\Phi_q = (\Phi_{sol} - \Phi_{agg})/\Phi_{sol}$, where Φ_{sol} and Φ_{agg} are the fluorescence emission quantum efficiency of the dye in dilute solution and in the aggregated state, respectively.[60] When f_w increases from 0 to 30%, Φ_F of *B*-PDI-ANQ drops from 54 to 2.8%. Φ_q is calculated to be as high as 95%. Under the same condition, Φ_F of *O*-PDI-ANQ decreases slowly from 70 to 60% and Φ_q is calculated to be 14%. Only at a very high f_w of 70%, Φ_F of *O*-PDI-ANQ decrease to 24% and Φ_q is calculated to be 66%. It is noted that the emission peak of *B*-PDI-ANQ gradually red-shifted from 570 to 645 nm when f_w is increased from 50 to 70%. This result indicates that the aggregation of *B*-PDI-ANQ involves intermolecularπ–π interactions, which would increase the coplanarity of the π-conjugated molecules and should result in a red-shift of the emission wavelength due to excimer formation.[61] Interestingly, the emission peak of *B*-PDI-ANQ shows a small blue-shift by approximately 5 nm at f_w = 80% as compared with that at f_w = 70%. The abnormal phenomenon of spectral shift is related to the degree of aggregation. When the degree of aggregation exceeds a certain range (f_w > 70%), the intermolecular π–π interactions are weakened rather than strengthened, leading to a blue-shift of the emission wavelength. A similar behavior of emission wavelength is also observed for *O*-PDI-ANQ.

Femtosecond transient absorption of *B*-PDI-ANQ and *O*-PDI-ANQ in THF/H_2O systems

According to the literature, on one hand, molecular aggregation could enhance the ISC rate and thereby suppressing fluorescence. This mechanism is termed "aggregation-induced intersystem crossing" (AI-ISC).[62,63] On the other hand, core-twist leads to an enhancement in triplet excited state generation, which is proposed as twisted π-conjugation-induced ISC.[64–68] The present study focuses on the impact of aggregation on the fluorescence properties of PDI derivatives in the core-twisted *vs.* planar conformation. The influence of the aggregation degree on the excited state is also tracked with the femtosecond transient absorption study. We choose aggregated *B*-PDI-ANQ in the THF/water mixture (with f_w of 30%) and *O*-PDI-ANQ in the

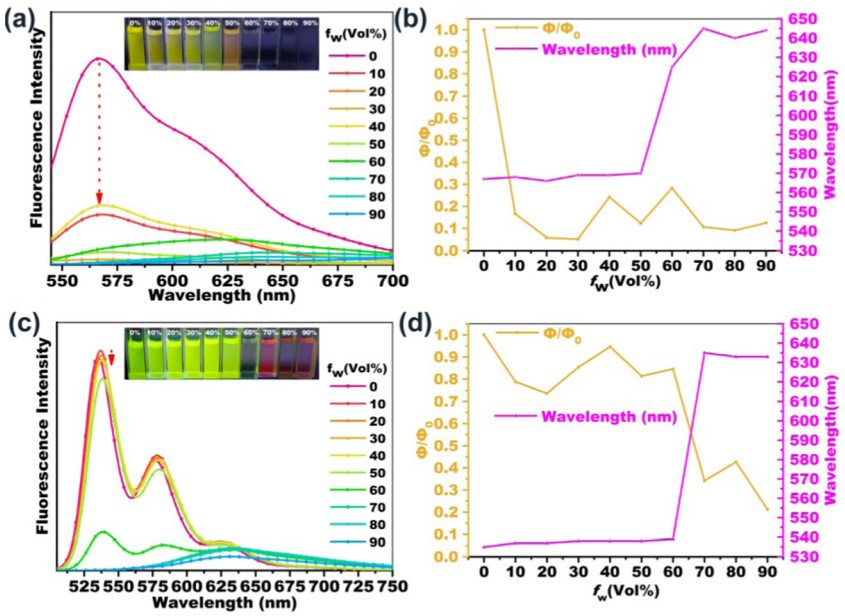

Fig. 3 The fluorescence emission spectra of (a) *B*-PDI-ANQ and (c) *O*-PDI-ANQ in the THF/water mixture with different water fractions (f_w). Variations of the fluorescence quantum yield and the maximum fluorescence emission wavelength for (b) *B*-PDI-ANQ and (d) *O*-PDI-ANQ in the THF/water mixture with different f_w. The insets of (a and c) show the photographs of FL images (taken under 365 nm UV light) for the corresponding mixtures.

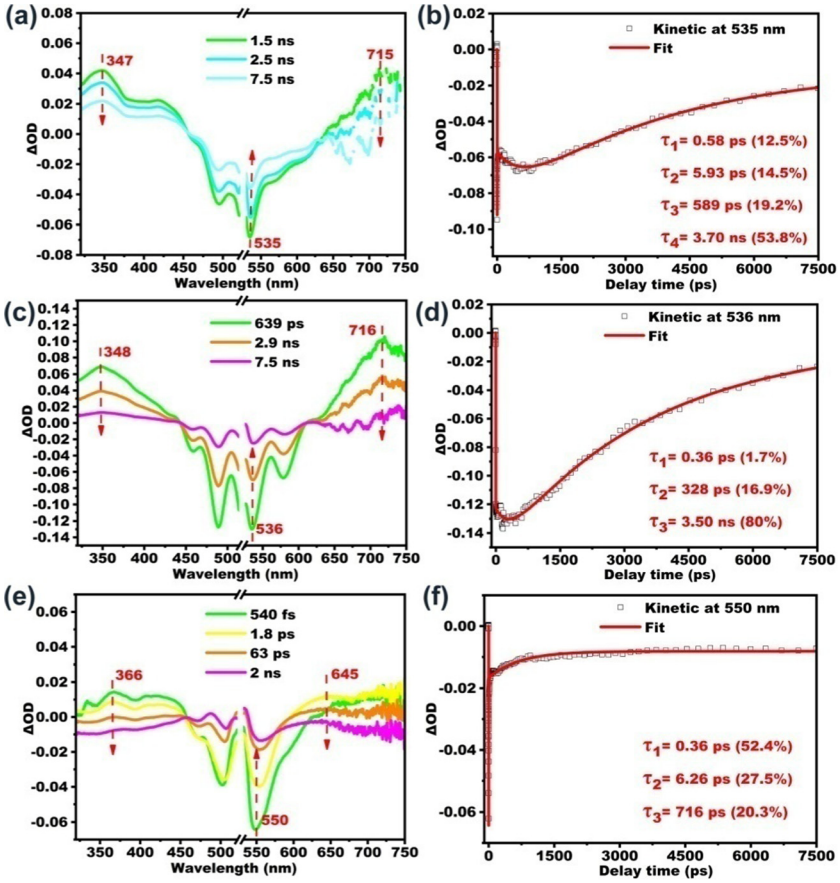

Fig. 4 Fs-TA spectra of (a) *B*-PDI-ANQ in THF/H_2O (f_w = 30%) and (c and e) *O*-PDI-ANQ in THF/H_2O (f_w = 30% and 70%) and (b, d and f) kinetics fitting at the corresponding wavelengths.

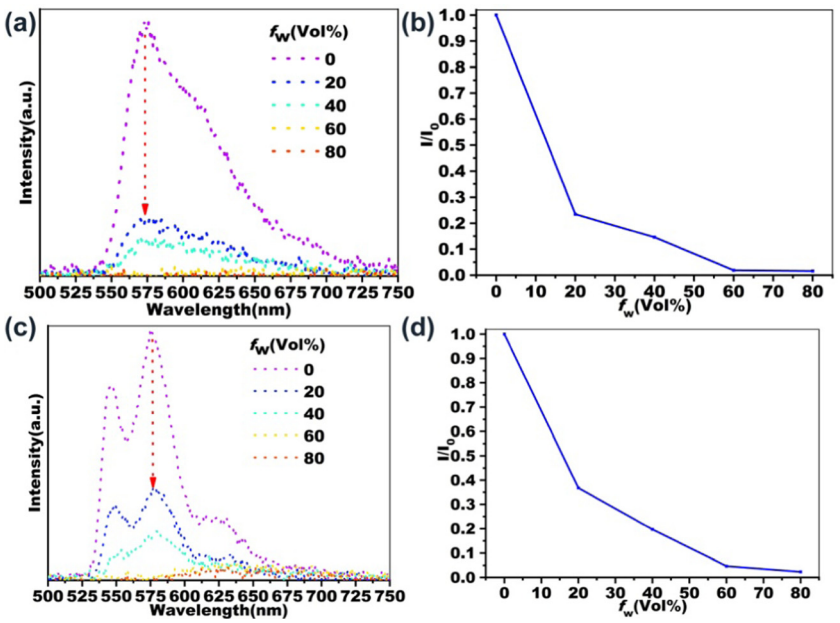

Fig. 5 Two-photon excited FL spectra of (a) *B*-PDI-ANQ and (c) *O*-PDI-ANQ in the THF/water mixture with different water fraction (f_w). Variation of 2PEF intensity for (b) *B*-PDI-ANQ and (d) *O*-PDI-ANQ in THF/water mixture with different f_w.

THF/water mixture (with f_w of 30% and 70%, respectively) as the test samples. As shown in Fig. 4, GSB and ESA bands show an apparent redshift upon aggregation. Four or three components are required for the satisfactory fitting of the data for *B*-PDI-ANQ and *O*-PDI-ANQ, respectively. At f_w = 30%, the ISC rate or the triplet rise time of aggregated *B*-PDI-ANQ is 3.70 ns, which is much shorter than that of non-aggregated *B*-PDI-ANQ (τ_{ISC} = 7.32 ns), while the ISC takes 3.50 ns in aggregated *O*-PDI-ANQ, which is only slightly shorter than that in non-aggregated *O*-PDI-ANQ (τ_{ISC} = 4.07 ns). Thus, aggregated *B*-PDI-ANQ displays a large fluorescence quenching at f_w = 30%, but aggregated *O*-PDI-ANQ only exhibits a small one. At f_w = 70%, the ISC takes 716 ps in aggregated *O*-PDI-ANQ, which is much shorter than that in non-aggregated *O*-PDI-ANQ. Therefore, the fluorescence of aggregated *O*-PDI-ANQ begins to quench largely then.

Two-photon excited fluorescence properties

The influence of aggregation on the two-photon excited fluorescence properties of PDI derivatives has also been investigated. As shown in Fig. 5, the two-photon excited fluorescence emission spectra of *B*-PDI-ANQ and *O*-PDI-ANQ in THF/H_2Omixtures with different water fractions are recorded. Interestingly, *B*-PDI-ANQ and *O*-PDI-ANQ all show fluorescence quenching with the increasing water fractions; however, there is some variation in the extent of the decline. To quantitatively describe their fluorescence quenching process, the changes in the I/I_0 values are plotted against the water fraction in the THF solutions. I_0 is the fluorescence intensity in THF. I is the fluorescence intensity in THF/H_2O mixtures. The tendencies are very clear: the fluorescence intensity of *B*-PDI-ANQ decreases relatively fast, with only 23% and 15% of its initial emission at f_w = 20% and f_w = 40%, respectively. The fluorescence intensity of *O*-PDI-ANQ shows a relatively slow but apparent decrease since it keeps 37% and 20% of its initial emission at f_w = 20% and f_w = 40%, respectively.

Cellular imaging

Banking on their bright emission, cellular imaging ability of *B*-PDI-ANQ and *O*-PDI-ANQ were assessed. Before this study, the cytotoxicity of the two PDI derivatives toward HeLa cells was tested. Results in Fig. 6a and b demonstrate that both *B*-PDI-ANQ and *O*-PDI-ANQ display negligible influence on the viability of HeLa cells, indicating a good biocompatibility of these two PDI derivatives. Then, cells are incubated with *B*-PDI-ANQ or *O*-PDI-ANQ for 8 h. A commercially available probe Lyso-tracker blue (LTB) with lysosome targetability is used for indicating

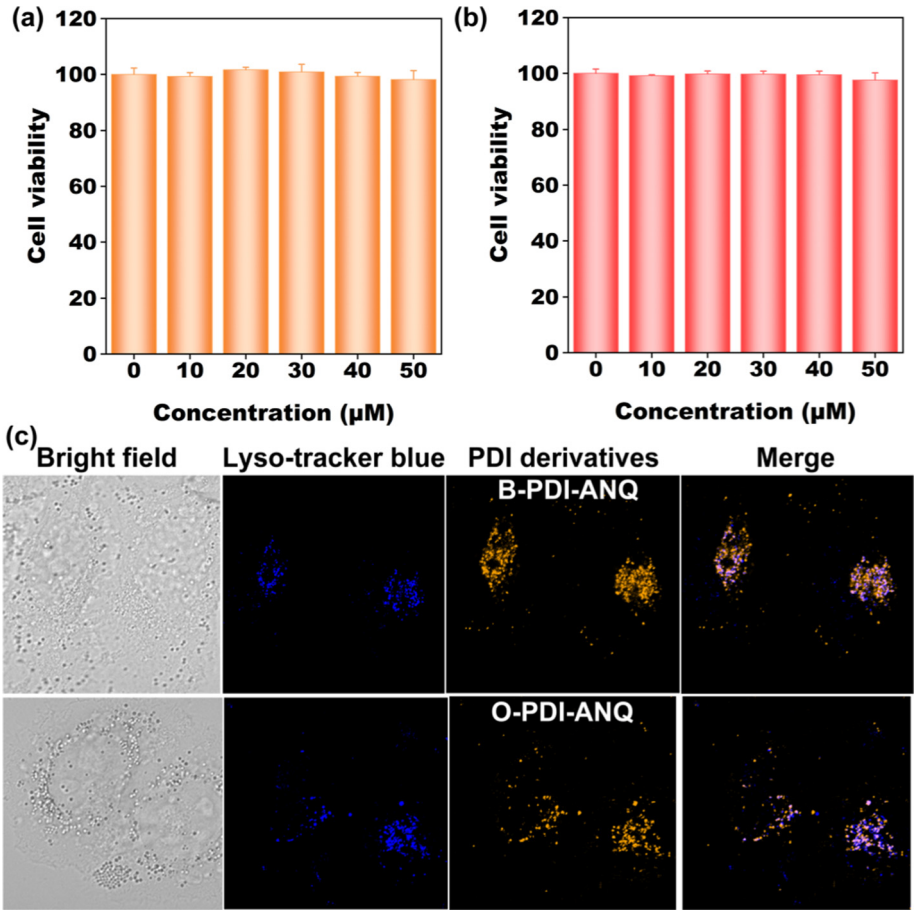

Fig. 6 (a and b) Cell viability of HeLa cells incubated with different concentrations of *B*-PDI-ANQ and *O*-PDI-ANQ for 8 h. (c) Confocal images of HeLa cells co-stained with *B*-PDI-ANQ and *O*-PDI-ANQ (25 μM) and LTB (25 μM).

cellular lysosomes. As displayed in Fig. 6c, both *B*-PDI-ANQ and *O*-PDI-ANQ exhibit bright orange emission inside cells and the bright emission matches well with the blue emission of probe Lyso-tracker blue, verifying the lysosome-targeting capability of *B*-PDI-ANQ and *O*-PDI-ANQ. These data confirm the potential application of *B*-PDI-ANQ and *O*-PDI-ANQ in fluorescence imaging of live cells and further visualization of biological procedures that occur inside lysosomes.

Conclusions

In summary, the regioisomerism strategy is employed in exploring the structure–property relationship of aggregated PDI derivatives. The experimental and theoretical results reveal that changing the substitution position of the anthraquinone group on the PDI from the *bay* position to the *ortho* position can improve the planarity of the PDI core and enhance the structural rigidity of the product. Femtosecond transient absorption studies on their isolated and aggregated state confirm that the regioisomerism from the *bay* to the *ortho* position not only blocks the nonradiative decay channels in the non-aggregated state but also decelerates nonradiative excited-state decay in the aggregated state, thus resulting in enhanced fluorescence emission of the isolated molecules and a suppressed fluorescence quenching effect of the aggregated molecules. Two-photon excited fluorescence studies on their aggregated state also show a suppressed fluorescence quenching effect of the *ortho*-substituted product. Cellular imaging studies reveal their potential application in fluorescence imaging of live cells.

Conflicts of interest

There are no conflicts to declare.

Acknowledgements

This work was supported by the National Natural Science Foundation of China (52073167, 21702132) and the Guangdong Basic and Applied Basic Research Foundation (2021A1515011879). Q. Z. thanks the funding support from the City University of Hong Kong (9380117, 7005620 and 7020040) and Hong Kong Institute for Advanced Study, City University of Hong Kong, Hong Kong, P.R. China.

Notes and references

1 M. Fang, J. Yang and Z. Li, *Prog. Mater. Sci.*, 2022, **125**, 100914.
2 (*a*) D. Ding, D. Mao, K. Li, X. Wang, W. Qin, R. Liu, D. S. Chiam, N. Tomczak, Z. Yang, B. Z. Tang, D. Kong and B. Liu, *ACS Nano*, 2014, **8**, 12620–12631; (*b*) Y. Huang, J. Xing, Q. Gong, L.-C. Chen, G. Liu, C.-J. Yao, Z. Wang, H.-L. Zhang, Z. Chen and Q. Zhang, *Nat. Commun.*, 2019, **10**, 169; (*c*) P. Gu, Z. Wang and Q. Zhang, *J. Mater. Chem. B*, 2016, **4**, 7060–7074.
3 J. Qi, C. Sun, D. Li, H. Zhang, W. Yu, A. Zebibula, J. W. Y. Lam, W. Xi, L. Zhu, F. Cai, P. Wei, C. Zhu, R. T. K. Kwok, L. L. Streich, R. Prevedel, J. Qian and B. Z. Tang, *ACS Nano*, 2018, **12**, 7936–7945.
4 L. Zong, H. Zhang, Y. Li, Y. Gong, D. Li, J. Wang, Z. Wang, Y. Xie, M. Han, Q. Peng, X. Li, J. Dong, J. Qian, Q. Li and Z. Li, *ACS Nano*, 2018, **12**, 9532–9540.
5 J. Wang, X. Gu, P. Zhang, X. Huang, X. Zheng, M. Chen, H. Feng, R. T. K. Kwok, J. W. Y. Lam and B. Z. Tang, *J. Am. Chem. Soc.*, 2017, **139**, 16974–16979.
6 R. Tang and Z. Li, *Chem. Rec.*, 2017, **17**, 71–89.
7 L. Xu, H. Zhu, G. Long, J. Zhao, D. Li, R. Ganguly, Y. Li, Q.-H. Xu and Q. Zhang, *J. Mater. Chem. C*, 2015, **3**, 9191–9196.
8 L. Xu and Q. Zhang, *Sci. China Mater.*, 2017, **60**, 1093.
9 L. Xu, J. Zhang, L. Yin, X. Long, W. Zhang and Q. Zhang, *J. Mater. Chem. C*, 2020, **8**, 6342–6349.
10 L. Xu, W. Lin, B. Huang, J. Zhang, X. Long, W. Zhang and Q. Zhang, *J. Mater. Chem. C*, 2021, **9**, 1520–1536.
11 A. Huang, Q. Li and Z. Li, *Chin. J. Chem.*, 2022, **40**, 2356–2370.
12 J. Yang, M. Fang and Z. Li, *Aggregate*, 2020, **1**, 6–18.
13 Q. Li and Z. Li, *Sci. China Mater.*, 2020, **63**, 177–184.
14 J. Luo, Z. Xie, J. W. Y. Lam, L. Cheng, H. Chen, C. Qiu, H. S. Kwok, X. Zhan, Y. Liu, D. Zhu and B. Z. Tang, *Chem. Commun.*, 2001, 1740–1741.
15 J. Yang, X. Zhen, B. Wang, X. Gao, Z. Ren, J. Wang, Y. Xie, J. Li, Q. Peng, K. Pu and Z. Li, *Nat. Commun.*, 2018, **9** 840.
16 H. Zhang, Z. Zhao, A. T. Turley, L. Wang, P. R. McGonigal, Y. Tu, Y. Li, Z. Wang, R. T. K. Kwok, J. W. Y. Lam and B. Z. Tang, *Adv. Mater.*, 2020, **32**, 2001457.
17 Q. Li and Z. Li, *Acc. Chem. Res.*, 2020, **53**, 962–973.
18 C. Wang, B. Xu, M. Li, Z. Chi, Y. Xie, Q. Li and Z. Li, *Mater. Horiz.*, 2016, **3**, 220–225.
19 J. Wang, Z. Chai, J. Wang, C. Wang, M. Han, Q. Liao, A. Huang, P. Lin, C. Li, Q. Li and Z. Li, *Angew. Chem., Int. Ed.*, 2019, **58**, 17297–17302.
20 (*a*) B. Xu, J. He, Y. Mu, Q. Zhu, S. Wu, Y. Wang, Y. Zhang, C. Jin, C. Lo, Z. Chi, A. Lien, S. Liu and J. Xu, *Chem. Sci.*, 2015, **6**, 3236–3241; (*b*) Z. Wang, F. Yu, W. Chen, J. Wang, J. Liu, C.-J. Yao, J. Zhao, H. Dong, W. Hu and Q. Zhang, *Angew. Chem., Int. Ed.*, 2020, **59**, 17580–17586.
21 M. Fang, J. Yang, Q. Liao, Y. Gong, Z. Xie, Z. Chi, Q. Peng, Q. Li and Z. Li, *J. Mater. Chem. C*, 2017, **5**, 9879–9885.
22 F. Liu, J. Tu, X. Wang, J. Wang, Y. Gong, M. Han, X. Dang, Q. Liao, Q. Peng, Q. Li and Z. Li, *Chem. Commun.*, 2018, **54**, 5598–5601.
23 Y. Yu, Y. Fan, C. Wang, Y. Wei, Q. Liao, Q. Li and Z. Li, *J. Mater. Chem. C*, 2019, **7**, 13759–13763.
24 X. Jia, C. Shao, X. Bai, Q. Zhou, B. Wu, L. Wang, B. Yue, H. Zhu and L. Zhu, *Proc. Natl. Acad. Sci. U. S. A.*, 2019, **116**, 4816–4821.
25 M. Louis, H. Thomas, M. Gmelch, A. Haft, F. Fries and S. Reineke, *Adv. Mater.*, 2019, **31**, 1807887.
26 L. Gu, H. Shi, M. Gu, K. Ling, H. Ma, S. Cai, L. Song, C. Ma, H. Li, G. Xing, X. Hang, J. Li, Y. Gao, W. Yao, Z. Shuai, Z. An,

X. Liu and W. Huang, *Angew. Chem., Int. Ed.*, 2018, **57**, 8425–8431.
27 Q. Dang, L. Hu, J. Wang, Q. Zhang, M. Han, S. Luo, Y. Gong, C. Wang, Q. Li and Z. Li, *Chem. – Eur. J.*, 2019, **25**, 7031–7037.
28 Y. Wang, J. Yang, M. Fang, Y. Gong, J. Ren, L. Tu, B. Z. Tang and Z. Li, *Adv. Funct. Mater.*, 2021, **31**, 2101719.
29 Z. A. Li, Z. Li, C. A. Di, Z. Zhu, Q. Li, Q. Zeng, K. Zhang, Y. Liu, C. Ye and J. Qin, *Macromolecules*, 2006, **39**, 6951–6961.
30 Z. a Li, Q. Zeng, Z. Li, S. Dong, Z. Zhu, Q. Li, C. Ye, C. a Di, Y. Liu and J. Qin, *Macromolecules*, 2006, **39**, 8544–8546.
31 Z. a Li, W. Wu, G. Yu, Y. Liu, C. Ye, J. Qin and Z. Li, *ACS Appl. Mater. Interfaces*, 2009, **1**, 856–863.
32 W. Wu, Q. Huang, G. Qiu, C. Ye, J. Qin and Z. Li, *J. Mater. Chem.*, 2012, **22**, 18486–18495.
33 W. Wu, C. Wang, R. Tang, Y. Fu, C. Ye, J. Qin and Z. Li, *J. Mater. Chem. C*, 2013, **1**, 717–728.
34 W. Wu, C. Ye, J. Qin and Z. Li, *ACS Appl. Mater. Interfaces*, 2013, **5**, 7033–7041.
35 R. Tang, S. Zhou, Z. Cheng, G. Yu, Q. Peng, H. Zeng, G. Guo, Q. Li and Z. Li, *Chem. Sci.*, 2017, **8**, 340–347.
36 Q. Li and Z. Li, *Adv. Sci.*, 2017, **4**, 1600484.
37 G. Jiang, R. Hu, C. Li, J. Gong, J. Wang, J. W. Y. Lam, A. Qin and B. Zhong Tang, *Chem. – Eur. J.*, 2022, DOI: **10.1002/chem.202202388**.
38 Y. Zhou, W. Qin, C. Du, H. Gao, F. Zhu and G. Liang, *Angew. Chem., Int. Ed.*, 2019, **58**, 12102–12106.
39 Y. Fan, Q. Li and Z. Li, *Mater. Chem. Front.*, 2021, **5**, 1525–1540.
40 J. Yang, H. Gao, Y. Wang, Y. Yu, Y. Gong, M. Fang, D. Ding, W. Hu, B. Z. Tang and Z. Li, *Mater. Chem. Front.*, 2019, **3**, 1391–1397.
41 Y. Yu, Y. Fan, C. Wang, Y. Wei, Q. Liao, Q. Li and Z. Li, *Mater. Chem. Front.*, 2021, **5**, 817–824.
42 M. Fang, J. Yang, X. Xiang, Y. Xie, Y. Dong, Q. Peng, Q. Li and Z. Li, *Mater. Chem. Front.*, 2018, **2**, 2124–2129.
43 S. Sasaki, K. Igawa and G.-I. Konishi, *J. Mater. Chem. C*, 2015, **3**, 5940–5950.
44 Y. Yu, C. Wang, Y. Wei, Y. Fan, J. Yang, J. Wang, M. Han, Q. Li and Z. Li, *Adv. Opt. Mater.*, 2019, **7**, 1900505.
45 H. Wu, X. Song, B. Zhang, Z. Wang, T. Zhang, A. Qin and B. Z. Tang, *Mater. Chem. Front.*, 2020, **4**, 1706–1713.
46 Y. Li, S. Liu, H. Ni, H. Zhang, H. Zhang, C. Chuah, C. Ma, K. S. Wong, J. W. Y. Lam, R. T. K. Kwok, J. Qian, X. Lu and B. Z. Tang, *Angew. Chem., Int. Ed.*, 2020, **59**, 12822–12826.
47 P. Funchien, P. Chasing, T. Sudyoadsuk and V. Promarak, *Chem. Commun.*, 2020, **56**, 6305–6308.
48 L. R. Adil and P. K. Iyer, *Chem. Commun.*, 2020, **56**, 7633–7636.
49 H.-X. Yu, J. Zhi and J.-L. Wang, *J. Mater. Chem. C*, 2021, **9**, 3882–3891.
50 Q. Zhao, S. Zhang, Y. Liu, J. Mei, S. Chen, P. Lu, A. Qin, Y. Ma, J. Z. Sun and B. Z. Tang, *J. Mater. Chem.*, 2012, **22**, 7387–7394.
51 X. Long, J. Wu, S. Yang, Z. Deng, Y. Zheng, W. Zhang, X.-F. Jiang, F. Lu, M.-D. Li and L. Xu, *J. Mater. Chem. C*, 2021, **9**, 11679–11689.
52 L. Xu, X. Long, F. Kang, Z. Deng, J. He, S. Yang, J. Wu, L. Yin, X.-F. Jiang, F. Lu, M.-D. Li and Q. Zhang, *J. Mater. Chem. C*, 2022, **10**, 7039–7048.
53 B. Carlotti, I. K. Madu, H. Kim, Z. Cai, H. Jiang, A. K. Muthike, L. Yu, P. M. Zimmerman and T. Goodson, *Chem. Sci.*, 2020, **11**, 8757–8770.
54 H. Zhu, Y. Yang, K. Wu and T. Lian, *Annu. Rev. Phys. Chem.*, 2016, **67**, 259–281.
55 S. Yamaguchi and H.-O. Hamaguchi, *J. Chem. Phys.*, 1998, **109**, 1397–1408.
56 I. H. M. van Stokkum, D. S. Larsen and R. van Grondelle, *Biochim. Biophys. Acta, Bioenerg.*, 2004, **1657**, 82–104.
57 S. J. Formosinho and L. G. Arnaut, *J. Photochem. Photobiol., A*, 1993, **75**, 21–48.
58 J. H. Lee, M. Wulff, S. Bratos, J. Petersen, L. Guerin, J.-C. Leicknam, M. Cammarata, Q. Kong, J. Kim, K. B. Møller and H. Ihee, *J. Am. Chem. Soc.*, 2013, **135**, 3255–3261.
59 P. Foggi, L. Bussotti and F. V. R. Neuwahl, *Int. J. Photoenergy*, 2001, **3**, 164849.
60 Y. J. Wang, Z. Li, J. Tong, X. Y. Shen, A. Qin, J. Z. Sun and B. Z. Tang, *J. Mater. Chem. C*, 2015, **3**, 3559–3568.
61 Y. Liu, Y. Zhang, X. Wu, Q. Lan, C. Chen, S. Liu, Z. Chi, L. Jiang, X. Chen and J. Xu, *J. Mater. Chem. C*, 2014, **2**, 1068–1075.
62 L. Yang, X. Wang, G. Zhang, X. Chen, G. Zhang and J. Jiang, *Nanoscale*, 2016, **8**, 17422–17426.
63 J. Zhang, E. Sharman, L. Yang, J. Jiang and G. Zhang, *J. Phys. Chem. C*, 2018, **122**, 25796–25803.
64 K. Nagarajan, A. R. Mallia, V. S. Reddy and M. Hariharan, *J. Phys. Chem. C*, 2016, **120**, 8443–8450.
65 K. Nagarajan, A. R. Mallia, K. Muraleedharan and M. Hariharan, *Chem. Sci.*, 2017, **8**, 1776–1782.
66 Z. Mahmood, A. A. Sukhanov, N. Rehmat, M. Hu, A. Elmali, Y. Xiao, J. Zhao, A. Karatay, B. Dick and V. K. Voronkova, *J. Phys. Chem. B*, 2021, **125**, 9317–9332.
67 Y. Dong, B. Dick and J. Zhao, *Org. Lett.*, 2020, **22**, 5535–5539.
68 Z. Wang, L. Huang, Y. Yan, A. M. El-Zohry, A. Toffoletti, J. Zhao, A. Barbon, B. Dick, O. F. Mohammed and G. Han, *Angew. Chem., Int. Ed.*, 2020, **59**, 16114–16121.

